

 Open access • Journal Article • DOI:10.1086/500636

350 μm dust emission from high-redshift quasars — [Source link](#)

[Alexandre Beelen](#), [Alexandre Beelen](#), [Pierre Cox](#), [Dominic J. Benford](#) ...+5 more authors

Institutions: [University of Bonn](#), [Max Planck Society](#), [Goddard Space Flight Center](#), [Jet Propulsion Laboratory](#) ...+3 more institutions

Published on: 10 May 2006 - [The Astrophysical Journal](#) (American Astronomical Society)

Topics: [Luminous infrared galaxy](#), [Quasar](#), [Caltech Submillimeter Observatory](#), [Spectral energy distribution](#) and [Redshift](#)

Related papers:

- [350 Micron Dust Emission from High Redshift Quasars](#)
- [Dust emission from the most distant quasars](#)
- [Star formation in galaxies along the hubble sequence](#)
- [STAR FORMATION AND GAS KINEMATICS OF QUASAR HOST GALAXIES AT \$z \sim 6\$: NEW INSIGHTS FROM ALMA](#)
- [Thermal emission from warm dust in the most distant quasars](#)

Share this paper:    

View more about this paper here: <https://typeset.io/papers/350-mm-dust-emission-from-high-redshift-quasars-1v2204nybt>

350 μm DUST EMISSION FROM HIGH-REDSHIFT QUASARS

ALEXANDRE BEELEN

Institut d’Astrophysique Spatiale, Bâtiment 121, Université de Paris XI, F-91405 Orsay, France; Max-Planck-Institut für Radioastronomie, Auf dem Hügel 69, D-53121 Bonn, Germany; and Radioastronomisches Institut der Universität Bonn, Auf dem Hügel 71, D-53121 Bonn, Germany; alexandre.beelen@ias.u-psud.fr

PIERRE COX

Institut de Radioastronomie Millimétrique, St. Martin d’Heres, F-38406, France; cox@iram.fr

DOMINIC J. BENFORD

NASA Goddard Space Flight Center, Code 665, Greenbelt, MD 20771; dominic.benford@nasa.gov

C. DARREN DOWELL

Jet Propulsion Laboratory, Mail Code 169-506, Pasadena, CA 91109; cdd@submm.caltech.edu

ATTILA KOVÁCS

California Institute of Technology, MS 320-47, Pasadena, CA 91125; attila@submm.caltech.edu

FRANK BERTOLDI

Radioastronomisches Institut Universität Bonn, Auf dem Hügel 71, 53121 Bonn, Germany; bertoldi@astro.uni-bonn.de

ALAIN OMONT

Institut d’Astrophysique de Paris, CNRS, and Université de Paris VI, 98bis Boulevard Arago, F-75014 Paris, France; omont@iap.fr

AND

CHRIS L. CARILLI

National Radio Astronomy Observatory, P.O. Box O, Socorro, NM 87801; ccarilli@aoc.nrao.edu

Received 2005 September 26; accepted 2005 December 6

ABSTRACT

We report detections of six high-redshift ($1.8 \leq z \leq 6.4$), optically luminous, radio-quiet quasars at 350 μm , using the SHARC II bolometer camera at the Caltech Submillimeter Observatory. Our observations double the number of high-redshift quasars for which 350 μm photometry is available. By combining the 350 μm measurements with observations at other submillimeter/millimeter wavelengths, for each source we have determined the temperature of the emitting dust (ranging from 40 to 60 K) and the far-infrared luminosity $[(0.6\text{--}2.2) \times 10^{13} L_{\odot}]$. The combined mean spectral energy distribution of all high-redshift quasars with two or more rest-frame far-infrared photometric measurements is best fit with a graybody with temperature of 47 ± 3 K and a dust emissivity power-law spectral index of $\beta = 1.6 \pm 0.1$. This warm dust component is a good tracer of the starburst activity of the quasar host galaxy. The ratio of the far-infrared to radio luminosities of infrared-luminous, radio-quiet high-redshift quasars is consistent with that found for local star-forming galaxies.

Subject headings: galaxies: evolution — galaxies: starburst — infrared: galaxies — infrared: ISM — quasars: individual (APM 08279+5255, HS 1002+4400, KUV 08086+4037, J1409+5628, PSS 2322+1944, SDSS J1148+5251)

Online material: color figures

1. INTRODUCTION

At high redshifts, a large fraction of the star formation occurs in very luminous ($>10^{12} L_{\odot}$) galaxies (Greve et al. 2005). Most of the radiation of the newly formed stars in these systems is absorbed by the dust and reemitted at infrared (IR) wavelengths. In their rest frame, the spectral energy distribution (SED) of dusty galaxies typically peaks at 60–80 μm and can be approximated with a modified blackbody spectrum with dust temperatures between 30 and 80 K (Dunne et al. 2000). In host galaxies of quasi-stellar objects (QSOs), some dust can be directly heated by the central active galactic nucleus (AGN) to higher temperatures; its emission then dominates the near- to mid-IR SED. For sources at high redshift ($z > 1$), the peak of the emission is shifted to submillimeter wavelengths, enabling useful multicolor photometric observations with ground-based telescopes in the submillimeter and millimeter atmospheric windows. Tracing the peak

of their SED is crucial for an accurate determination of the IR luminosity and star formation rate in such dusty, energetic systems.

In principle, a determination of the SED peak could be expected to be useful for estimating the source redshift in cases in which spectroscopic redshifts are not available. While this method has been shown to work in limited Monte Carlo simulations (Wiklind 2003; Hughes et al. 2002), there is the distinct possibility that it may be impractical, as the redshift and dust temperature are largely degenerate (Blain et al. 2003). Sampling the SED of high-redshift IR-luminous galaxies through the several submillimeter and millimeter atmospheric windows (usually 350, 450, 850 μm and 1.2, 2.0, 3.0 mm) has been achieved for only a few high- z sources (Benford et al. 1999; Priddey & McMahon 2001, and references therein).

Here we present observations at 350 μm of six quasars in the redshift range $1.8 \lesssim z \lesssim 6.4$. This doubles the number of high- z quasars for which such measurements are available. The optically

TABLE 1
OBSERVATIONAL PARAMETERS

Source	z	M_B	R.A. (J2000.0)	Decl. (J2000.0)	$S_{1.2\text{mm}}$ (mJy, $\pm 1\sigma$)	$S_{350\mu\text{m}}$ (mJy, $\pm 1\sigma^a$)	Integration Time (minutes)
KUV 08086+4037	1.78	-27.0	8 12 00.41	+40 28 15.00	4.3 ± 0.8^d	69 ± 11	180
APM 08279+5255 ^b	3.91	-32.9	8 31 41.70	+52 45 17.35	24 ± 2^c	386 ± 32	20
HS 1002+4400	2.08	-28.3	10 05 17.45	+43 46 09.30	4.2 ± 0.8^d	77 ± 14	170
J1148+5251	6.42	-28.4	11 48 16.64	+52 51 50.30	5.0 ± 0.6^f	21 ± 6^c	430
J1409+5628	2.58	-28.4	14 09 55.56	+56 28 26.50	10.7 ± 0.6^e	112 ± 12	220
PSS 2322+1944	4.12	-28.1	23 22 07.25	+19 44 22.08	9.6 ± 0.5^g	79 ± 11	150

NOTE.—Units of right ascension are hours, minutes, and seconds, and units of declination are degrees, arcminutes, and arcseconds.

^a The absolute calibration uncertainty of 20% is not included in the quoted values.

^b For APM 08279+5255, the flux density measured at 450 μm with SHARC II is 342 ± 26 mJy.

^c The flux density for J1148+5251 is derived with a FWHM of $11''.5$.

^d Omont et al. (2003).

^e Irwin et al. (1998) at 1.35 mm.

^f Bertoldi et al. (2003a).

^g Omont et al. (2001).

luminous and radio-quiet quasars were selected from the 1.2 millimeter continuum surveys performed with the Max-Planck Millimeter Bolometer (MAMBO) array by Omont et al. (2001, 2003) and Bertoldi et al. (2003a; also see Table 1). The selected wavelength of 350 μm roughly corresponds to the peak in the SEDs of highly redshifted emission from dust with temperatures of 40–60 K. We adopt the concordance Λ -cosmology with $H_0 = 71 \text{ km s}^{-1} \text{ Mpc}^{-1}$, $\Omega_\Lambda = 0.73$, and $\Omega_m = 0.27$ (Spergel et al. 2003).

2. OBSERVATIONS

The measurements were made on 2004 January 6 and 7 at the 10.4 m Leighton telescope of the Caltech Submillimeter Observatory (CSO) on the summit of Mauna Kea, Hawaii, during excellent weather conditions, with stable zenith atmospheric opacities of 1.0 at 350 μm . We used the CSO bolometer camera, SHARC II, described by Dowell et al. (2003), mounted at the reimaged Cassegrain focus. It consists of a 12×32 array of doped silicon “pop-up” bolometers operating at 350 μm . Under good weather conditions, the point-source sensitivity at 350 μm is $\sim 1 \text{ Jy (Hz)}^{-1/2}$ or better. The detectors of SHARC II cover the focal plane with 90% filling factor and are separated by $0.70\lambda/D = 4''.86$.

Pointing was checked regularly on strong sources including planets and secondary calibrators, and the focus was checked at the beginning of each night. The pointing was found to be stable with a typical accuracy of $\lesssim 2''$ (1σ rms). We used the Dish Surface Optimization System (DSOS), which actively corrects the 10.4 meter primary surface for static imperfections and deformations due to gravitational forces as the dish moves in elevation (Leong 2005). The DSOS improves the beam shape and provides an elevation-independent telescope efficiency $\sim 10\%$ better than the passive telescope (which has an aperture efficiency of 33% at 350 μm) at intermediate elevation and 50% better at high elevation. The beam of the CSO at 350 μm is approximated by a circular Gaussian with a FWHM of $8''.5$. Uranus served as a primary flux calibrator and the asteroids Pallas and Ceres as secondary calibrators. At the time of the observations, the brightness temperature of Uranus was 64 K and its diameter $3''.4$, corresponding to a 350 μm flux density of 224 Jy. The secondary calibrators Pallas, Ceres, and IRC +10216 had 350 μm flux densities of 7.0, 40, and 24 Jy, respectively, as derived by various observation made with SHARC II using Mars, Uranus, and Neptune as primary calibrators, with uncertainties of 15% based on repeat-

ability of observations. The absolute calibration was found to be accurate to within 20% at 95% confidence.

SHARC II was also used at 450 μm to observe APM 08279+5255 on 2004 January 13, 16, and 18 under good weather conditions ($\tau_{225 \text{ GHz}} \sim 0.09$). For these observations, we used as the secondary calibrators Ceres and IRC +10216, which had flux densities at 450 μm of 28 and 13 Jy, respectively.

The observations were performed by scanning the SHARC II array in azimuth and elevation using Lissajous and box-scan patterns with amplitudes of $15''.0 \times 14''.14$ and $25''.0 \times 35''.22$, respectively, in order to reduce systematic errors. The SHARC II array is rectangular, of $2''.61 \times 0''.96$ in extent, with the long axis oriented in azimuth. The sources were also observed at different elevations before and after transit. The final maps have typical sizes of $\approx 2 \times 1 \text{ arcmin}^2$. At 350 μm , the total integration time per map is between 150 and 430 minutes, with the exception of APM 08276+5255, which was observed for only 20 minutes. The corresponding rms map noise values are in the range from 5 to 15 mJy (Table 1).

The data were reduced using version 1.42 of the software package CRUSH (Comprehensive Reduction Utility for SHARC II; G. Kovács 2006, in preparation). CRUSH is based on an algorithm that solves a series of models that try to reproduce the observations through an iterative process, taking into account instrumental and atmospheric effects while using statistical estimators on the data. For the current data, we used the option deep, which is appropriate for sources with typical flux densities smaller than 1 Jy beam^{-1} . To derive the flux densities of the high- z quasars at 350 and 450 μm , we fitted circular Gaussians profiles and a uniform background level, leaving the position, the full width at half-maximum and the intensities as free parameters. The resulting noise maps were used to derive the statistical uncertainties on the fitted parameters that served to estimate the uncertainty on the flux densities. These uncertainties do not take into account the calibration errors.

3. RESULTS

All six quasars were detected at significance levels higher than $\sim 3.5\sigma$ (Table 1). The signal maps of the 350 μm continuum emission are shown in Figure 1. In the following, we comment on the individual sources.

KUV 08086+4037.—This $z = 1.78$ broad emission line quasar was discovered by Darling & Wegner (1996) and detected at 1.2 mm by Omont et al. (2003). The millimeter to 1.4 GHz

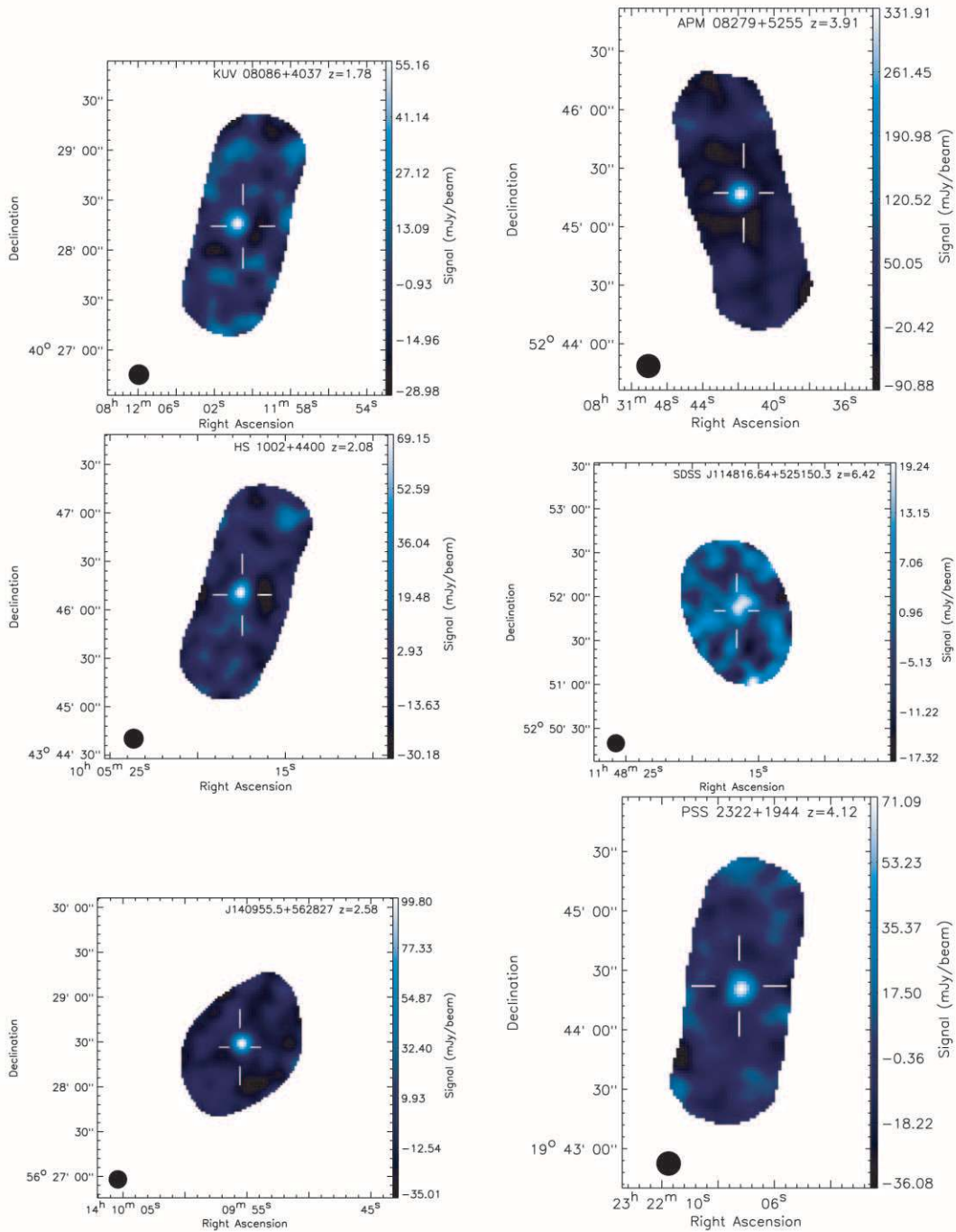


FIG. 1.—SHARC II maps at $350\ \mu\text{m}$ of the six optically luminous, radio-quiet high- z quasars studied in this paper. The names and redshifts are given in the top left corner of each panel. The maps have been cut to half of the maximum exposure and smoothed with a $9''$ FWHM Gaussian. The resulting beam size is shown in the bottom left corner of each plot. The crosses indicate the optical positions of the quasars as listed in Table 1.

radio continuum flux ratio is compatible with a star-forming galaxy (Petric et al. 2004). We detect KUV 08086+4037 at $350\ \mu\text{m}$ with a flux density of 69 ± 11 mJy. The peak emission of KUV 08086+4037 is shifted by 3 to $\sim 4''$ from the optical or radio position, corresponding to $\sim 2\ \sigma$ of the pointing accuracy of the CSO. However, it is unlikely that the detected emission does not come from the QSO, and the offset is probably due to a pointing model problem.

APM08279+5255.—This is a strongly lensed $z = 3.91$ broad absorption line quasar with a bolometric luminosity of $\sim 10^{14} L_{\odot}$ after correction for magnification by a factor of 7 (Downes et al.

1999). It is a strong IR/submillimeter source that was even detected by the *Infrared Astronomical Satellite (IRAS)* (Irwin et al. 1998). Its mid-IR spectrum was observed with the *Spitzer Space Telescope*, confirming a strong continuum likely due to the dust heated by the AGN (Soifer et al. 2004). The massive reservoir of dust (a few $\sim 10^8 M_{\odot}$) and warm molecular gas ($3 \times 10^9 M_{\odot}$) associated with this quasar is distributed in a nuclear disk of radius 100–200 pc around the AGN and traces a dynamical mass of $1.5 \times 10^{10} M_{\odot}$ (Lewis et al. 2002). With a $350\ \mu\text{m}$ flux density of 386 ± 32 mJy, APM 8279+5255 is the strongest high- z source ever detected at $350\ \mu\text{m}$. The flux density at $450\ \mu\text{m}$ measured

with SHARC II is 342 ± 26 mJy and was found to be stable over the three different observations periods, 319 ± 32 mJy on January 13, 279 ± 111 mJy on the 16th and 418 ± 52 mJy on the 18th. This flux density is higher than the 211 ± 47 (68) mJy reported by Lewis et al. (1998) and the 285 ± 11 (40) mJy found by Barvainis & Ivison (2002), but is still compatible with them within 1σ , when taking into account the absolute calibration uncertainties of SCUBA, as quoted in parenthesis and estimated to be of the order of 10%.

HS 1002+4400.—This is a quasar at $z = 2.08$ that was first discovered in the Hamburg survey (Hagen et al. 1999). It displays broad emission lines with no peculiar features, and it was detected at 1.2 millimeter by Omont et al. (2003) and in the 1.4 GHz radio continuum by Petric et al. (2004). The radio to millimeter continuum flux ratio is consistent with that of a starburst. HS 1002+4400 is detected at 350 μm with a flux density of 77 ± 14 mJy.

SDSS J114816.64+5251.—This object, hereafter referred to as J1148+5251, is the most distant quasar ($z = 6.42$) known to date (Fan et al. 2003). An optically very luminous quasar, powered by a supermassive black hole, it also shows strong far-IR emission with an estimated luminosity of $1.2 \times 10^{13} L_{\odot}$ (Bertoldi et al. 2003a) and an implied rate of star formation of $\approx 3000 M_{\odot} \text{ yr}^{-1}$. A massive reservoir of dense molecular gas ($\approx 2 \times 10^{10} M_{\odot}$) is implied by the observed CO emission (Walter et al. 2003; Bertoldi et al. 2003b) and the recent detection of the [C II] emission line (Maiolino et al. 2005). The 1.4 GHz radio continuum flux follows the radio-FIR correlation for star-forming galaxies (Carilli et al. 2004). J1148+5251 as been detected both at 850 and 450 μm by Robson et al. (2004), with flux densities of 7.8 ± 0.7 and 24.7 ± 7.4 mJy, respectively. Charmandaris et al. (2004) reported the detection of J1148+5251 with the *Spitzer Space Telescope* at 16 and 22 μm , revealing a hot dust component that could be heated by the AGN; however, it should be noted that these measurement are also compatible with the emission of the AGN extrapolated from the optical. We detected J1148+5251 at 350 μm with a flux density of 21 ± 6 mJy at the optical position of the QSO. This is the lowest flux density ever detected at 350 μm . A map with the best-fit source subtracted presents only noise, with any residual sources < 14 mJy, meaning that the apparent source extension seen in Figure 1 is due to noise.

J140955.5+562827.—This object, hereafter referred to as J1409+5628, at $z = 2.56$ is an optically very bright, radio-quiet quasar. It is by far the strongest millimeter source in the Omont et al. (2003) MAMBO survey of $z \approx 2$ quasars. It has a massive reservoir of warm and dense molecular gas that is detected in CO (Beelen et al. 2004) and HCN (Carilli et al. 2005), with an estimated mass of $6 \times 10^{10} M_{\odot}$. Its far-IR luminosity of $\sim 4 \times 10^{13} L_{\odot}$ implies a star formation rate of several 1000 $M_{\odot} \text{ yr}^{-1}$ (Beelen et al. 2004). The radio flux density is consistent with the radio-FIR correlation for star-forming galaxies (Petric et al. 2004). High-resolution VLBA observations resolve out the radio emission, implying an intrinsic brightness temperature of $\sim 10^5$ K at 8 GHz, which is typical for nuclear starbursts (Beelen et al. 2004). The 350 μm flux density of 112 ± 12 mJy places J1409+5628 among the strongest submillimeter high- z sources.

PSS 2322+1944.—This is an optically luminous, lensed (magnification $a = 3.5$) quasar at $z = 4.12$. It was detected in millimeter dust and radio continuum, and in various CO emission lines (Omont et al. 2001; Cox et al. 2002; Carilli et al. 2002). With a far-IR luminosity of $9 \times 10^{12} L_{\odot}$ (corrected for lensing), it harbors a massive reservoir of molecular gas detected in CO, where star formation takes place with a rate of $\approx 1000 M_{\odot} \text{ yr}^{-1}$. The CO line emission is resolved into an Einstein ring, which can be modeled

as a disk of dense and warm molecular gas surrounding the QSO with a radius of ~ 2 kpc, tracing a dynamical mass of a few $10^{10} M_{\odot}$ (Carilli et al. 2003). PSS 2322+1944 is clearly detected at 350 μm with a flux density of 79 ± 11 mJy.

4. DISCUSSION

The thermal emission from dust at a temperature T_{dust} , is proportional to $B_{\nu}(T_{\text{dust}})(1 - e^{-\tau_d})$, where $B_{\nu}(T_{\text{dust}})$ is the Planck function and $\tau_d(\lambda) = \kappa(\lambda) \int \rho ds$ is the dust optical depth, with κ being the mass absorption coefficient at rest wavelength λ and ρ the total mass density. At far-IR wavelengths $\lambda > 40 \mu\text{m}$, the emission is optically thin, $\tau_d \ll 1$, so that the above expression applied to a given dust mass at redshift z leads to an emergent flux density

$$S_{\nu_0} = \frac{(1+z)}{D_L^2} M_{\text{dust}} \kappa(\nu_r) B_{\nu_r}(T_{\text{dust}}) \quad (1)$$

$$\propto \nu_r^{3+\beta} \frac{1}{\exp(h\nu_r/kT_{\text{dust}}) - 1}, \quad (2)$$

where the mass absorption coefficient, $\kappa(\nu) = \kappa_0(\nu/\nu_0)^{\beta}$, is approximated by a power law.

Dusty galaxies typically show multitemperature components in their IR SEDs. At rest-frame near- and mid-IR wavelengths, the emission from these quasars arises from a “hot” (several 100 K) but not very massive dust component, that is likely heated directly by the AGN. The far-IR emission, on the other hand, arises from starburst regions where most of the energy emerges from dust with temperatures in the range 30–80 K, but by mass, most of the dust could be in a 10–20 K component that is energetically overpowered by the warmer component.

Through a fit of a single-temperature graybody (three free parameters: luminosity or integrated intensity, β , and T_{dust}), the dust temperature and emissivity index can be determined simultaneously only if *at least* four photometric data points are available (fit with more than one degree of freedom). For most objects, only two photometric data points (S_1 and S_2 at ν_1 and ν_2) are available, resulting in a degeneracy between the dust temperature and β (Priddey & McMahon 2001; Blain et al. 2003):

$$\alpha e^{h\nu_1/kT_{\text{dust}}} - e^{h\nu_2/kT_{\text{dust}}} = \alpha - 1, \quad (3)$$

where $\alpha = (\nu_2/\nu_1)^{3+\beta} S_1/S_2$.

4.1. Individual Objects

We fit a modified black-(gray)body spectrum (eq. [1]) to the rest-frame 40–800 μm SEDs of the six high- z quasars we observed at 350 μm . To account for the uncertainties in the absolute calibration of the submillimeter and millimeter photometry, we added 20% to the uncertainties of all measurements.

For those quasars for which only two photometric data points are available, we fixed $\beta = 1.6$ (see § 4.2) and derived T_{dust} from equation (3). When more photometric measurements are available, we performed a χ^2 fit on T_{dust} only, or both T_{dust} and β when the number of degrees of freedom in the fit was greater than 1, except in the case of J1148+5251, where the lack of detection in the Rayleigh-Jeans domain prevent the fit of β . The resulting fits are shown in Figure 2 for four of the quasars for which three or more measurements are available. Figure 2 also shows the available radio, near- and mid-IR measurements, as well as the radio continuum emission expected from the correlation between the far-IR and radio luminosity observed in nearby star-forming galaxies (Condon 1992).

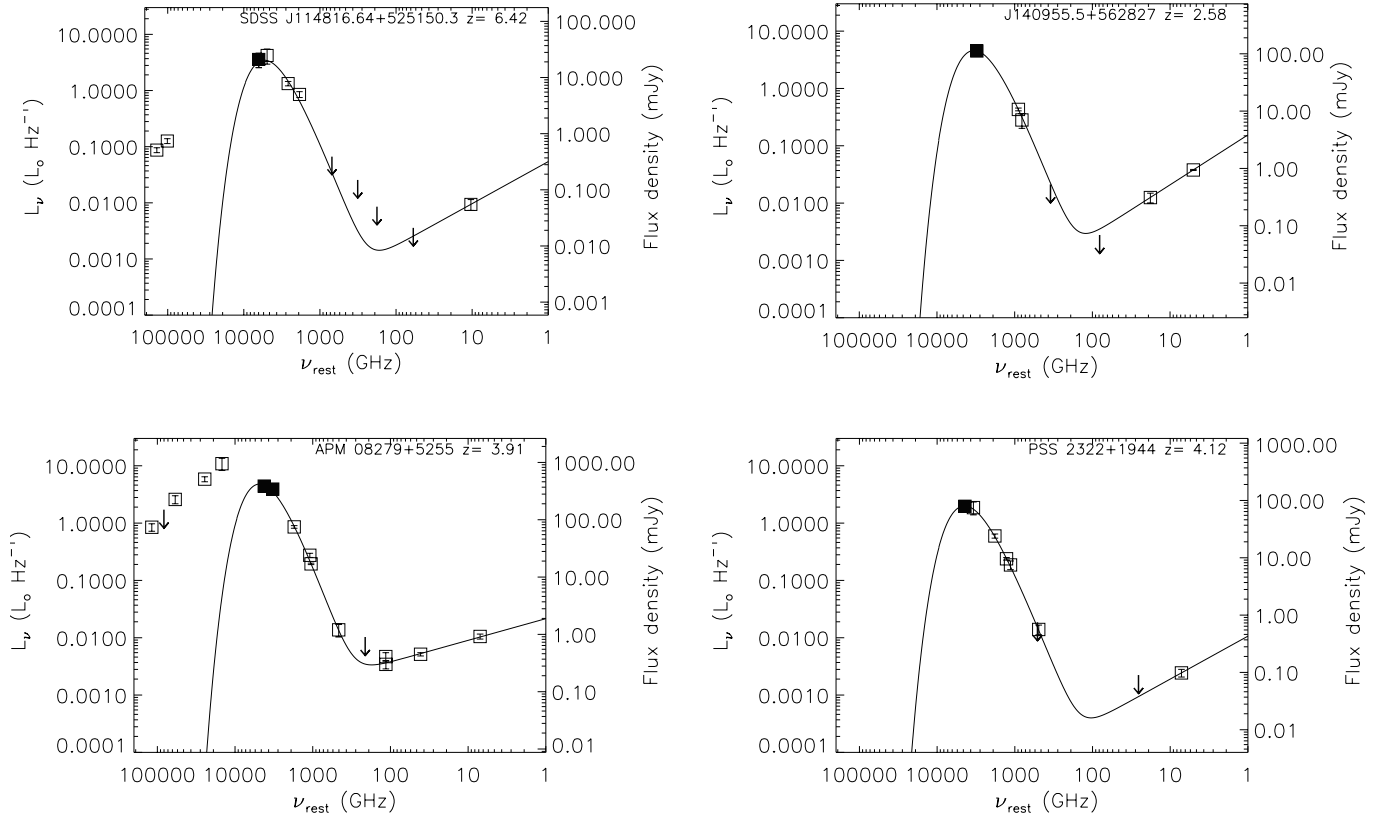


FIG. 2.—Spectral energy distributions (SEDs) of J1148+5251, J1409+5628, APM 08279+5255, and PSS 2322+1944 in the rest frame of the sources. The SHARC II 350 and 450 μm points are shown as filled squares. Other measurements (taken from the literature) are displayed with open squares, with arrows indicating 3σ upper limits. The solid line shows the best fit to the far-IR data using a modified blackbody and to the radio using a power law (see text and parameters in Table 2). When needed the radio spectral index was set to 0.75. The references to the photometric measurements other than from SHARC II are J1148+5251: Bertoldi et al. (2003a); Carilli et al. (2003, 2004); Robson et al. (2004); Charmandaris et al. (2004); J1409+5628: Omont et al. (2003); Beelen et al. (2004); Petric et al. (2004); PSS 2322+1944: Cox et al. (2002) and references therein; and APM 08279+5255: Irwin et al. (1998); Lewis et al. (1998, 2002); Downes et al. (1999). [See the electronic edition of the Journal for a color version of this figure.]

The far-IR luminosity is found by integrating over the fitted modified blackbody. The mass M_{dust} of dust at T_{dust} is related to far-IR luminosity by

$$L_{\text{FIR}} = 4\pi M_{\text{dust}} \int \kappa(\nu) B_{\nu}(T_{\text{dust}}) d\nu, \quad (4)$$

or to the flux density $S_{\nu_{\text{obs}}}$ observed at frequency ν_{obs} (see eq. [1])

A major source of uncertainty in estimating the dust mass comes from uncertainties of the mass absorption coefficient κ , which is poorly constrained by observations or laboratory ex-

periments. We adopt a value of $0.4 \text{ cm}^2 \text{ g}^{-1}$ at $1200 \mu\text{m}$, which is in the range of values found in the literature (Alton et al. 2004 and references therein). For each source, the derived temperature, spectral index, luminosity, and dust mass are listed in Table 2.

The dust spectral index could be fitted for only two of our sources, APM 08279+5255 and PSS 2322+1944, resulting in $\beta = 1.9 \pm 0.3$ and 1.5 ± 0.3 , respectively. The fixed value of $\beta = 1.6$ for the other sources is based on the mean SED discussed in § 4.2. Our values are consistent with those found for dusty local galaxies: $1.3 \leq \beta \leq 2.0$ (Dunne et al. 2000; Priddey & McMahon 2001; Alton et al. 2004, and references therein) and

TABLE 2
DERIVED PROPERTIES

Source	T_{dust} (K)	β	Amplification Factor	L_{FIR} ($10^{13} L_{\odot}$)	Dust Mass ($10^8 M_{\odot}$)	q
KUV 08086+4037	32 ± 5	1.6^{a}	...	0.6 ± 0.3	23.8	2.1 ± 0.2
APM 08279+5255	47 ± 7	1.9 ± 0.3	7^{b}	2.7 ± 0.7	5.7	$2.6 \pm 0.1^{\text{c}}$
HS 1002+4400.....	38 ± 7	1.6^{a}	...	1.2 ± 0.7	17.3	...
J1148+5251.....	55 ± 5	1.6^{a}	...	2.2 ± 0.7	4.2	2.2 ± 0.2
J1409+5628.....	35 ± 2	1.6^{a}	...	1.9 ± 0.4	48.6	$1.6 \pm 0.1^{\text{d}}$
PSS 2322+1944.....	47 ± 8	1.5 ± 0.3	3.5^{e}	1.1 ± 0.3	6.8	2.5 ± 0.1

NOTE.—The far-IR luminosities and dust masses are corrected for lensing amplification when indicated.

^a Fixed value.

^b From Lewis et al. (2002).

^c Where $\alpha_{\text{radio}} = -0.35 \pm 0.07$.

^d Where $\alpha_{\text{radio}} = -1.0 \pm 0.1$.

^e From Carilli et al. (2003).

are slightly lower than the $\beta = 2$ expected for pure silicate and/or graphite grains (Draine & Lee 1984).

The derived temperatures for the warm dust are in the range 30–60 K, which is typical for local IR-luminous galaxies, where the heating is dominated by young, massive stars (Dunne et al. 2000). The values are also comparable to those found for other high- z sources (Benford et al. 1999). Our single-component fits do not account for the hot dust component that dominates at rest-frame mid-IR wavelengths. For APM 08279+5255, e.g., when adopting $\beta = 1.9$, a two dust component fit to the SED between 10 and 800 μm yields $T_{\text{hot}} = 155 \pm 17$ K and $T_{\text{warm}} = 45 \pm 2$ K. The warm dust temperature agrees well with the value found from a single dust component fit. The situation is similar for the Cloverleaf, where a single-component fit yields $T_{\text{dust}} = 38 \pm 3$ K and $\beta = 2.0 \pm 0.2$, whereas a two-component fit with fixed $\beta = 2$ yields $T_{\text{hot}} = 118 \pm 13$ K and $T_{\text{warm}} = 36 \pm 1$ K, which also agrees with the results of Weiß et al. (2003). The same applies in the case of IRAS F10214+4724 with a single-component fit yields to $T_{\text{dust}} = 44 \pm 7$ K with β fixed to 1.6, and a two-component fit to $T_{\text{hot}} = 93 \pm 12$ K and $T_{\text{warm}} = 41 \pm 8$ K. These three examples (see Fig. 3) suggest that the temperatures found for the warm dust from single-component fits are not much affected by the hot dust component—although this probably depends somewhat on the relative intensities of both components. Further measurements at the rest-frame peak emission, from 10 to 100 μm , are needed to clearly solve this problem. Note that a dust temperature distribution is more likely to be found, instead of a single component or two dust components.

The derived dust masses range from a few times 10^8 to $10^9 M_{\odot}$ (Table 2), indicating huge reservoirs of gas in the high- z quasars. However, uncertainties in these mass estimates arise from the assumed value of the mass absorption coefficient κ , which is constrained only within a factor of 4 (Alton et al. 2004). Furthermore, there may well be a cold dust component for which emission would remain hidden below that of the warm component even if it contained up to three times the mass of the warm component (Dunne et al. 2000; Dunne & Eales 2001).

4.2. Dust Temperature and Spectral Index of the Mean Far-IR SED of High- z Quasars

The determination of both β and T_{dust} is currently possible only for a few objects. Even when enough photometric data points are available for individual sources, the uncertainties on the temperature and the spectral index are large and the $\beta - T_{\text{dust}}$ degeneracy prevents reliable estimates of the far-IR luminosities.

To better constrain the mean properties of the high-redshift quasar warm dust component, we have fitted a single-temperature graybody to the photometric points of all quasars with at least two measurements in the rest-frame far-IR. This provides a useful empirical description of the mean far-IR SED of dusty high- z galaxies, which can be used as a template to derive the far-IR luminosities when only a few photometric measurements are available. The 14 quasars of this sample have redshifts in the range 1.8–6.4, which provides a “wavelength coverage” of the ensemble SED much wider than that possible for individual objects. Figure 4 shows the resulting mean SED.

A similar analysis was done by Priddey & McMahon (2001) for a smaller sample of $z > 4$ quasars, where they found $T_{\text{dust}} = 41 \pm 5$ K and $\beta = 1.95 \pm 0.3$. Instead of iteratively normalizing the SEDs, we left the normalization of each SED a free parameter in the combined fit. Thereby no prior assumption is made on the scale, but each source SED needs two or more far-IR flux measurements to bring at least 1 degree of freedom to the fit. The best-fit values, $T_{\text{dust}} = 47 \pm 3$ K, $\beta = 1.6 \pm 0.1$, the χ^2

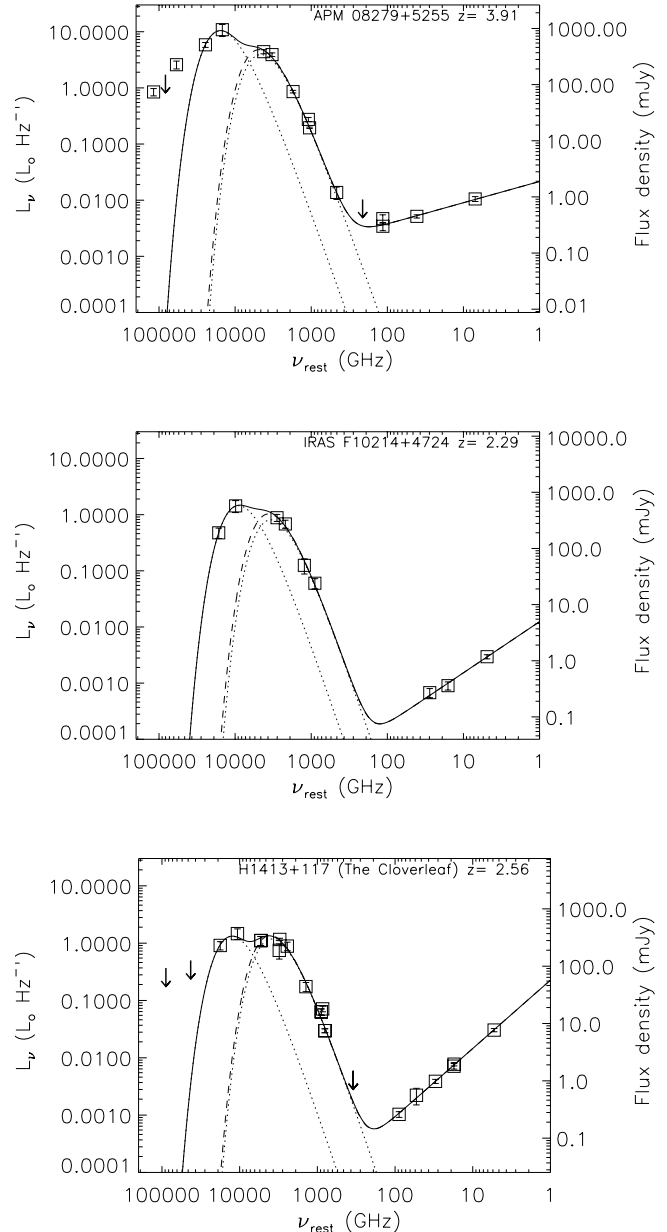


FIG. 3.—SEDs of APM 08279+5255, IRAS 10214+4724, and the Cloverleaf in the rest frame of the sources. The solid line shows the best fit to the mid-/far-IR data using two-component models (solid and dotted lines) and to the radio using a power law (see text for parameters). The dashed line corresponds to a single-component fit to the far-IR data. [See the electronic edition of the *Journal* for a color version of this figure.]

contours, and the $\beta - T_{\text{dust}}$ degeneracy are shown in Figure 5. The fitted SED is overplotted on the ensemble of scaled measurements in Figure 4. Although consistent (within 1σ) with the results of Priddey & McMahon (2001), our findings suggest a somewhat higher dust mean temperature and lower β .

The derived mean spectral index of $\beta = 1.6 \pm 0.1$ is not consistent with the value of $\beta = 2$ expected for dust grains made of pure silicates and/or graphites (Draine & Lee 1984). However, a range of dust temperatures will lower the effective measured β . For example, the sum of two modified blackbodies with dust temperatures T_{warm} and T_{cold} and $\beta = 2$ provides a fit to the mean far-IR SED that is as good as the one with a single dust temperature and $\beta = 1.5$ (see also Dunne & Eales 2001). The mean value of $\beta = 1.6$ was adopted in § 4.1 to fit the dust temperature for sources

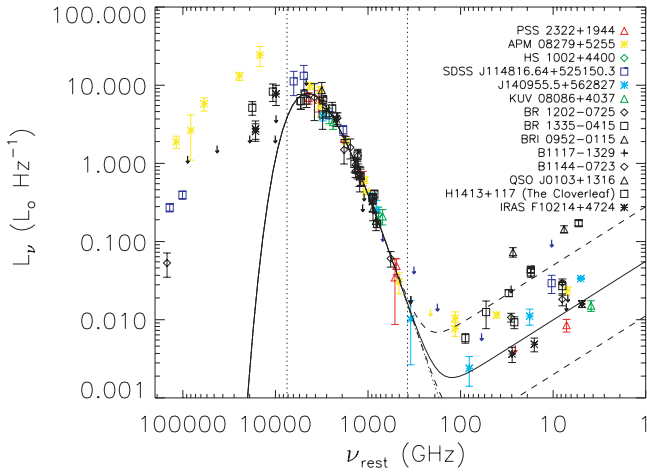


FIG. 4.—Combined SED, in the rest frame, for all the high- z quasars from this paper and sources discussed in Benford et al. (1999) and Priddey & McMahon (2001; see references therein and in our Fig. 2). The SEDs have been normalized to the far-IR luminosity of PSS 2322+1944. Each quasar is represented with a different symbol, identified in the panel. The best fit to the rest-frame far-IR data together with the derived radio continuum are shown using the same definitions as in Fig. 2. The corresponding dust temperature and spectral index are displayed in Fig. 5. The two vertical dot-dashed lines delineate the wavelength domain defined as the far-IR in this paper.

with only a few photometric measurements. The current data do not well constrain an additional cold component, for which measurements at longer wavelengths, 2–3 mm, would be most valuable.

4.3. Infrared to Radio Spectral Index

For local star-forming galaxies a tight linear correlation is found between the radio continuum (monochromatic) luminosity, $L_{1.4\text{ GHz}}$, and the far-IR luminosity, L_{FIR} , with a scatter of a factor ≈ 2 –3 over more than 4 orders of magnitude in luminosity (Condon 1992; Yun et al. 2001). This tight relation is generally understood to be due to star-formation activity, measuring the dust heated by young stars, and the radio synchrotron emission from supernova remnants. That this relation also holds at higher

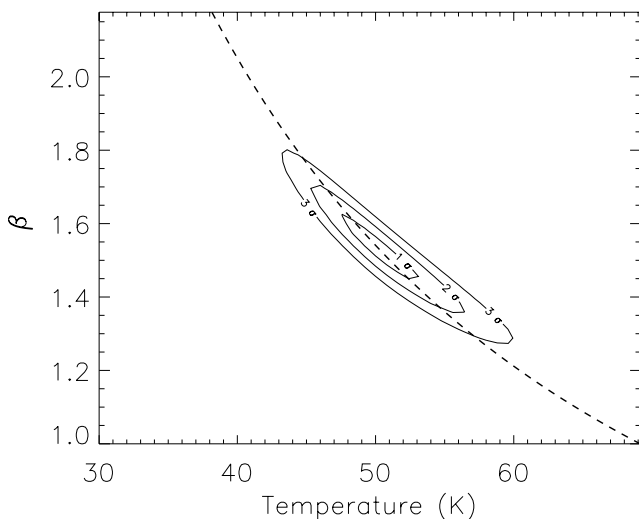


FIG. 5.—Contours of χ^2 in the β - T_{dust} plane for the combined SEDs of the high- z quasars shown in Fig. 4. Contours represent the 1, 2, and 3 σ uncertainties. The dashed line represents the β - T_{dust} degeneracy (see text for details). [See the electronic edition of the Journal for a color version of this figure.]

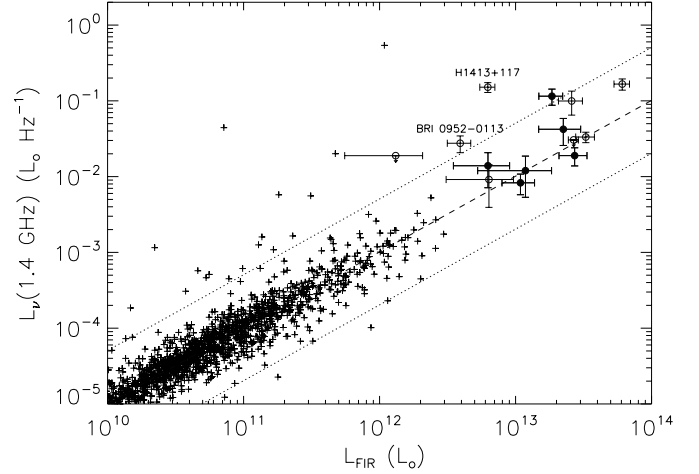


FIG. 6.—Rest-frame 1.4 GHz luminosity as a function of the L_{FIR} as defined by Condon (1992; see text). The crosses are for the *IRAS* 2 Jy sample of Yun et al. (2001) and the circles for the sources discussed in this paper that have radio detection (filled circles are sources from Table 1, whereas open circles are sources taken from the literature and listed in Fig. 4). The dashed line shows the mean value of q , while the dotted lines display the IR and radio excesses, which are 5 times above and below the value expected from the linear far-IR/radio relation. When known, the luminosities of the high- z sources have been corrected for lensing. [See the electronic edition of the Journal for a color version of this figure.]

redshifts was shown by Appleton et al. (2004), who report evidence for its validity out to $z = 2$ by matching *Spitzer Space Telescope* 24 and 70 μm sources and VLA (Very Large Array) radio sources. In the following, we check whether the Condon correlation also holds for high- z far-IR-luminous quasars.

The far-IR/radio relationship is usually quantified by a parameter

$$q \equiv \log\left(\frac{L_{\text{FIR}}}{3.75 \times 10^{12} \text{ W}}\right) - \log\left(\frac{L_{1.4\text{ GHz}}}{1 \text{ W Hz}^{-1}}\right), \quad (5)$$

where $L_{1.4\text{ GHz}}$ is the monochromatic rest-frame 1.4 GHz luminosity (Helou et al. 1985; Condon 1992) and L_{FIR} is the far-IR luminosity, which was originally computed from the rest-frame 60 and 100 μm *IRAS* fluxes (Helou et al. 1985) under the assumption of a typical dust temperature of ≈ 30 K. However, these definitions are not practical for ultraluminous infrared galaxies (ULIRGs) that have higher dust temperatures, and we therefore use the integrated far-IR luminosity of the warm dust component.

To compute the radio luminosities we fitted a power law to the observed radio flux densities and extrapolate to the rest-frame 1.4 GHz flux density. When only one data point is available, we use a radio spectral index of -0.75 (Condon 1992).

The resulting q values are listed in Table 2. Figure 6 plots the radio luminosity against the far-IR luminosity for the 2 Jy galaxy sample of Yun et al. (2001). To be consistent with our definitions, we recomputed the far-IR luminosities by fitting a single dust temperature modified blackbody with $\beta = 1.6$. The figure compares the Yun sample to the high- z quasars sample, except for HS 1002+4400, for which no radio data are available (see the caption of Fig. 6 for details).

Most of our quasars follow the far-IR/radio correlation well, showing a median $q = 2.2 \pm 0.4$, in good agreement with the value of 2.3 ± 0.1 found for the Yun sample. Two quasars show unusually high radio to far-IR flux ratios: BRI 0952–0115, which shows a radio luminosity similar to that of a low-luminosity radio galaxy (Yun et al. 2000), and the Cloverleaf, which contains a known weakly radio-loud AGN.

The fact that the high- z quasars reasonably follow the Condon relation for star-forming galaxies suggests that their radio and far-IR emission also arise from star formation, although a weak contribution from the AGN is not excluded. Further evidence for this is provided by the vast amounts of dense molecular gas detected in CO line emission for some of the quasars (see § 3) and by the implied several kpc spatial extent of these gas reservoirs, which is very similar to that of the starburst rings resolved in nearby Seyfert and starburst galaxies (García-Burillo et al. 2003).

5. CONCLUSIONS

This paper reports sensitive measurements of 350 μm dust emission from high-redshift quasars. The detection of six $1.8 \leq z \leq 6.4$ quasars doubles the number of quasars at high redshift for which 350 μm photometry is available. Combined with observations at mm/submillimeter wavelengths, the 350 μm data allow us to sample the rest-frame far-IR SEDs of these high- z sources and, thereby, to constrain the properties of their warm dust emission. The 350 μm measurements are key in deriving the far-IR luminosities since they sample the peak of the warm dust emission. For the high- z quasars, the derived temperatures are in the range 40–60 K, and the luminosities are a few $10^{13} L_{\odot}$. The derived dust masses range from a few times 10^8 to $10^9 M_{\odot}$.

The mean far-IR SED of all high- z quasars measured with two or more rest-frame far-IR data points is best fit with a graybody of temperature, $T_{\text{dust}} = 47 \pm 3$ K and a dust emissivity spectral index, $\beta = 1.6 \pm 0.1$. However, note that there are considerable variations and uncertainties in the determination of the dust temperature and spectral index in individual objects, which is not reflected in the quoted uncertainties here. To determine accurately β and T_{dust} , a good sampling of the SED, especially along the Rayleigh-Jeans part of the modified blackbody is needed with measurements around the emission peak. Photometric measurements at high-frequency (e.g., at 350 μm) are important to sample the peak of the redshifted far-IR emission and derive the far-IR luminosity, whereas data at low frequencies (2 or 3 mm)

would be key to constrain β . Future facilities such as the Atacama Large Millimeter Array (ALMA) will improve the sensitivity in the submillimeter/mm regime by more than an order of magnitude relative to current instrumentation and will enable the measurement of the SEDs of high- z sources over a wide range in frequency with a precise calibration, including much less luminous and extreme objects than the ones that can be observed today.

All the radio-quiet high- z quasars studied in this paper approximately follow the far-IR/radio correlation, showing a median $q = 2.2 \pm 0.4$, consistent with that found for local star-forming galaxies. This result is a further indication that, in these high- z radio-quiet quasars, the radio and far-IR emission does arise from star formation.

The warm (40–60 K) dust component found from single-component fits to the SEDs of high-redshift quasars is not much affected by the presence of a hot (several 100 K) dust component that dominates at rest-frame mid-IR wavelengths, as shown by the examples of APM 08279+5255 and the Cloverleaf. The warm dust component is thus found to be a relatively good tracer of the starburst activity of the quasars's host galaxy.

More mid-IR measurements are needed to assess the degree to which the warm and hot dust components can be treated independently in high- z quasars. In this respect, the *Spitzer Space Telescope* will provide valuable photometric data at mid-IR wavelengths and allow us to build complete SEDs for a number of high redshift quasars from their rest-frame near- to far-IR wavelengths to investigate the relative importance of the AGN and starburst activity.

The CSO is funded by the NSF under contract AST 02-29008. A. B. acknowledges financial support from the Programme National de Galaxies. We thank A. Jones and F. Boulanger for fruitful discussions on the subject of this work.

REFERENCES

- Alton, P. B., Xilouris, E. M., Misiriotis, A., Dasyra, K. M., & Dumke, M. 2004, *A&A*, 425, 109
- Appleton, P. N., et al. 2004, *ApJS*, 154, 147
- Barvainis, R., & Ivison, R. 2002, *ApJ*, 571, 712
- Beelen, A., et al. 2004, *A&A*, 423, 441
- Benford, D. J., Cox, P., Omont, A., Phillips, T. G., & McMahon, R. G. 1999, *ApJ*, 518, L65
- Bertoldi, F., et al. 2003a, *A&A*, 406, L55
- . 2003b, *A&A*, 409, L47
- Blain, A. W., Barnard, V. E., & Chapman, S. C. 2003, *MNRAS*, 338, 733
- Carilli, C. L., et al. 2002, *ApJ*, 575, 145
- . 2003, *Science*, 300, 773
- . 2004, *AJ*, 128, 997
- . 2005, *ApJ*, 618, 586
- Charmandaris, V., et al. 2004, *ApJS*, 154, 142
- Condon, J. J. 1992, *ARA&A*, 30, 575
- Cox, P., et al. 2002, *A&A*, 387, 406
- Darling, G. W., & Wegner, G. 1996, *AJ*, 111, 865
- Dowell, C. D., et al. 2003, *Proc. SPIE*, 4855, 73
- Downes, D., Neri, R., Wiklind, T., Wilner, D. J., & Shaver, P. A. 1999, *ApJ*, 513, L1
- Dunne, L., & Eales, S. A. 2001, *MNRAS*, 327, 697
- Dunne, L., Eales, S., Edmunds, M., Ivison, R., Alexander, P., & Clements, D. L. 2000, *MNRAS*, 315, 115
- Draine, B. T., & Lee, H. M. 1984, *ApJ*, 285, 89
- Fan, X., et al. 2003, *AJ*, 125, 1649
- García-Burillo, S., et al. 2003, *A&A*, 407, 485
- Greve, T. R., et al. 2005, *MNRAS*, 359, 1165
- Hagen, H.-J., Engels, D., & Reimers, D. 1999, *A&AS*, 134, 483
- Helou, G., Soifer, B. T., & Rowan-Robinson, M. 1985, *ApJ*, 298, L7
- Hughes, D. H., et al. 2002, *MNRAS*, 335, 871
- Irwin, M. J., Ibata, R. A., Lewis, G. F., & Totten, E. J. 1998, *ApJ*, 505, 529
- Leong, M. 2005, A CSO Submillimeter Active Optics System, in *Proc. URSI Commission J Meeting* (Chicago: Univ. Chicago), <http://astro.uchicago.edu/ursi-comm-j/ursi2005/rf-telescope-fabrication/leong/index.html>
- Lewis, G. F., Carilli, C., Papadopoulos, P., & Ivison, R. J. 2002, *MNRAS*, 330, L15
- Lewis, G. F., Chapman, S. C., Ibata, R. A., Irwin, M. J., & Totten, E. J. 1998, *ApJ*, 505, L1
- Maiolino, R., et al. 2005, *A&A*, 440, L51
- Omont, A., Beelen, A., Bertoldi, F., Cox, P., Carilli, C. L., Priddey, R. S., McMahon, R. G., & Isaak, K. G. 2003, *A&A*, 398, 857
- Omont, A., et al. 2001, *A&A*, 374, 371
- Petric, A., et al. 2004, *AJ*, submitted
- Priddey, R. S., & McMahon, R. G. 2001, *MNRAS*, 324, L17
- Robson, I., Priddey, R. S., Isaak, K., & McMahon, R. G. 2004, *MNRAS*, 351, L29
- Soifer, B. T., et al. 2004, *ApJS*, 154, 151
- Spergel, D. N., et al. 2003, *ApJS*, 148, 175
- Walter, F., et al. 2003, *Nature*, 424, 406
- Weiß, A., Henkel, C., Downes, D., & Walter, F. 2003, *A&A*, 409, L41
- Wiklind, T. 2003, *ApJ*, 588, 736
- Yun, M. S., Carilli, C. L., Kawabe, R., Tutui, Y., Kohno, K., & Ohta, K. 2000, *ApJ*, 528, 171
- Yun, M. S., Reddy, N. A., & Condon, J. J. 2001, *ApJ*, 554, 803